Preparation and Photoelectrochemistry of Semiconducting WS_2 Thin Films

D. Tonti, F. Varsano, and F. Decker*

Department of Chemistry, University "La Sapienza", 00185 Roma, Italy

C. Ballif,* M. Regula, and M. Remškar*

Institute of Applied Physics, Ecole Polytechnique Fédérale de Lausanne, 1015 Lausanne, Switzerland

Received: August 19, 1996[⊗]

Crystalline 2H-WS_2 thin films were prepared by thermal decomposition of amorphous WS_3 films sputter-deposited onto a thin Ni layer. Structural, electrical, and photoelectrochemical properties were investigated. Room temperature photoconductivity and photoelectrochemical response were shown to arise from the same interband transitions as in single crystals. The photocurrent spectra measured as a function of wavelength revealed a structure due to excitonic transitions. Surface modification by adsorption of ethylenediaminetetraacetic acid was shown to increase the photocurrent and to reduce the exciton recombination rate. A rectifying solid−liquid junction, having a barrier height of 0.45 V, was formed with the p-WS_2 films immersed in the aqueous $[Fe(CN)_6]^{3-/4-}$ redox electrolyte.

Introduction

Layered type materials are known to have very anisotropic physical properties. Transition metal dichalcogenides (TMDC) are layered materials which, owing to the low cohesive forces between layers, can be used for lubricating applications.[1] Moreover, TMDC samples in the form of single crystals have proven to be suitable for efficient and stable solar energy conversion devices.[2] TMDCs could be a viable alternative to other crystalline materials for photovoltaic cells provided a simple method for the growth of large surfaces of perfect single crystal would be available. This goal still seems to be far away, especially because of the purity of the available reagents.

Instead, in recent years new methods have been developed for the synthesis of thin TMDC films. Sputtered films typically exhibit platelets growing perpendicular to the substrate, on top of a dense thin layer with basal (00*n*) planes parallel to the substrate.[3,4] Such thin films are not well suited for electronic applications (solar cells) because of their irregular morphology and numerous stacking faults. Steps, edges of the platelets, and near-surface dislocations introduce electron states which are recognized to be preferential centers for the flow of dark current and for the recombination of photogenerated charge carriers.[5−7] Due to the shallow surface barrier for electron and holes, steps and edges act as a short circuit of the space charge layer in a semiconductor−metal (or semiconductor−electrolyte) junction.[8]

A novel method, combining the new growth technique introduced by Salitra et al.[9] and the thermal decomposition of WS_3, has been recently used to produce semiconducting, highly oriented WS_2 thin films with properties close to those of single crystals.[10] Such films could in principle be incorporated as the active electrode in photoelectrochemical solar cells. Photoelectrochemical solar cells based on WS_2 crystals have proven, in fact, to be reasonably efficient and durable.[11] Highly oriented thin films expose to the electrolyte chemically saturated chalcogenide atoms (the so-called Van der Waals planes), which are almost inactive, and only few steps and surfaces orthogonal to the van der Waals plans, where chalcogenide atoms and transition metals expose dangling bonds to the electrolyte.[5] Even working with highly oriented thin films, however, surface states and degenerated regions located mainly at grain boundaries have to be taken into account. Other technological problems to be solved, related to the fabrication process of solar cells, are the introduction of a metallic back contact and the passivation of the metallic phases still present in the films.

One way to improve the photoactivity of this class of highly oriented films would be to block the reactive sites and to passivate chemically the more conducting phases, provided the large part of the film surface has the exact stoichiometry and the proper morphology. Complexing species like ethylenediaminetetraacetic Acid (EDTA)[12] and semi-intercalating large molecules[13] have shown to be efficient passivating agents of single crystal electrodes; a reasonable passivation was obtained also with the electrochemically initiated polymerization of nonconductive polymers.[14] Transition metal atoms positioned on the reactive steps are thought to form coordination compounds with EDTA (and other complexing agents), and the passivation of the electrochemically most reactive surfaces could lead to a decrease of the dark current. Films treated with such complexing agents should show a definite improvement in their photoelectrochemical response because of the decrease of the photogenerated carrier recombination rate and of the increase of the shunt resistances in parallel with the junction. A different approach to the improvement of the photoactivity of this class of compounds by surface modification, the photoelectrochemical etching shown with WSe_2 by Tenne et al.,[15,16] although interesting, is not straightforward in our case due to the film thinness.

The aim of the work reported in this paper has been, therefore, to prepare samples of this novel film for a photoelectrochemical cell, and to test them both "as deposited" and after the application of surface treatments that could enhance the film photoresponse and the performance of the solid−liquid device.

Experimental Section

The preparation of the films consisted of a two-step process: (i) reactive rf sputtering at low substrate temperature (−10 to −20 °C) of an amorphous WS_3 layer (100 nm) on a quartz substrate covered with 10 nm evaporated nickel; (ii) annealing in argon flow (100 sccm, 5N7 purity) at 850 °C for 1 h.

* To whom correspondence should be addressed. E-mail: decker@axrma.uniromal.it; ballif@ipasg.epfl.ch.

⊗ Abstract published in *Advance ACS Abstracts,* March 1, 1997.

S1089-5647(96)02550-3 CCC: $14.00

TABLE 1: Deposition Parameters for Preparation of Amorphous WS_3 Films

target	WS_2 pressed powder
plasma gas	Ar + 5% H_2S
plasma pressure	1 Pa
substrate	quartz + Ni
substrate temp	−30 to −10 °C
Rf-power density	2 W/cm^2
deposition rate	1.2 Å/s
sample	**thickness (nm)**
85	200 (+7 nm Ni)
92b	100 (10 nm Ni)
72	100 (20 nm Ni)

The deposition was performed in a commercial magnetron rf-sputtering reactor. Main deposition parameters are summarized in Table 1. For the annealing step, the sample was introduced in the hot quartz tube stove at a speed of 1 cm/s and retracted at the same speed. This preparation method[10] allows the obtaining of highly oriented, photosensitive WS_2 films through thermal decomposition of WS_3 via the reaction $WS_3 \rightarrow W S_2 + S$. The excess sulfur either combines with nickel and forms NiS_x phases or is eliminated through the argon flow.

Nickel plays an essential role in the crystallization process as observed by Salitra et al.,[9] who proposed a model later called van der Waals rheotaxy.[17] This model states the presence of a NiS_x melt at the interface that acts as a flux medium, as in a rheotaxy process. Evidence for a catalytic growth mechanism is discussed in a recent publication,[18] where it is shown that Ni improves the crystallization at temperatures well below the eutectic point of the Ni−S phase and that the crystallization process is independent of the way the Ni is added. Films prepared by co-sputtering the Ni and the WS_3 phase show structural and electronic properties similar to the case where Ni is predeposited on the substrate. The morphology and the surface condition of the film have been studied by scanning electron microscopy (SEM) and in ultrahigh vacuum by scanning tunneling microscopy (STM). The structure of the annealed films was investigated by X-ray diffraction (XRD) in the $\theta-2\theta$ geometry. A film peeled off by immersion in a 1% HF solution has been deposited onto a copper grid for transmission electron microscopy (TEM) and for phase identification by means of selected area electron diffraction (SAD). Samples have been prepared for TEM cross-sectional views by mechanical polishing and ionic bombardment. The samples were carbonized to avoid charging effects. Ohmic gold contacts were evaporated on the annealed films for the electrical characterizations.

For photoelectrochemical experiments a layer of gold was evaporated on the film surface, leaving a free WS_2 surface exposed to the electrolyte in the form of a circle with an area of 10 mm^2. Metallic contact was established to the Au layer with a silver paste and was coated with commercial epoxy glue. The epoxy glue was used to mount the sample on a PVC substrate but proved to affect the conductivity of the film if not dried quickly at a temperature around 80 °C. The Au−semiconductor junction was always kept covered from light. Both electrochemical and photoelectrochemical experiments were performed in 0.5 M KCl, 10 mM $K_4Fe(CN)_6$, 10 mM $K_3Fe(CN)_6$ aqueous solution using two platinum wires as counter and reference electrodes.

In the photoelectrochemical experiments the distance between the mounted sample and the optical window was 1 cm. The sample area exposed both to the electrolyte and to the light was 10 mm^2. Electrochemical experiments were carried out with a 362 Princeton Applied Research potentiostat and a Mac II CI microcomputer controlled system. Impedance measurements were carried out with a Schlumberger Solartron 1255 HF frequency response analyzer (FRA); the frequency scanning interval was 0.1 Hz to 65 kHz. During cyclic voltammograms the samples were exposed to a 630 nm laser light chopped at 16 Hz, so that photocurrent could be followed as a function of the applied bias. A SR 530 Stanford Research System lock-in amplifier was used for Mott−Schottky plots (in the dark, with a 10 mV bias modulation at a 200 Hz frequency) and for photoelectrochemical measurements. Photocurrent spectra were recorded under chopped light using a white light source (tungsten halogen lamp) coupled to a monochromator (Applied Photophysics). Since linearity of the photocurrent with light intensity is satisfied only at low illumination levels, photoresponse measurements were performed in the presence of very weak external light and the photospectra were taken with a monochromatic beam with power less than 0.3 mW/cm^2.

Prolonged soaking of samples decreases photoactivities, and the best semiconducting behavior is shown if electrochemical characterizations are performed immediately after dipping the samples in the electrolyte. The WS_2 thin films were kept in contact with an aqueous solution of the disodium salt of EDTA (0.1 M) for periods varying from 1 h to 5 days at room temperature. Current−voltage curves under illumination and in the dark and photospectra were recorded again, and the results were then compared with those obtained previously with the same untreated film electrode. In order to repeat the experiments under the same illumination conditions, sample and cell were never removed from the optical bench; only reference and counter electrodes were withdrawn when the cell was filled with the EDTA solution and rinsed with distilled water.

Results and Discussion

(A) Structural and Optical Characterization. Figure 1a is a SEM image of the film surface. It shows WS_2 crystallites (A) with lateral sizes in the micrometer range and no preferred azimuthal orientation. Some needle crystallites (B) and occasional spherical grains (C) are also present. SAD analysis on the crystallites (inserts A−C) allows the identification of the different phases: the (A) platelets are WS_2 in its usual 2H polytypic modification (JCPDS:8−237). The B needles crystallites are $W_{18}O_{49}$ (JCPDS:36-101), resulting from partial oxidation with residual oxygen during annealing. The C droplets are nickel sulphide phases, mainly β-NiS grains (JCPDS:12-041); another weak Ni_3S_4 phase is detected. The surface of the WS_2 crystallites is almost defect free, and atomic resolution can be obtained on their surface by STM measurements, showing the hexagonal lattice of sulfur atoms (Figure 1b).

Figure 2 shows a typical XRD pattern of an annealed WS_3/Ni thin film. For comparison the XRD pattern of a WS_3 film annealed without the Ni layer is also represented, illustrating the drastic influence of the Ni layer on crystallinity. Figure 2 insert shows the decrease of the full width at half-maximum (fwhm) of the (002) reflection when the thickness of the Ni layer is increased, reaching with 7−10 nm Ni a lower limit of 0.17°, which is about the instrumental resolution of the diffractometer. On the XRD patterns, only (002*n*) peaks of 2H-WS_2 are present, indicating that the WS_2 crystallites are oriented with the *c*-axis perpendicular to the substrate. TEM cross-sectional views[19] of the WS_2 film confirm the perfect orientation of the film with the *c*-axis perpendicular to the substrate. It also shows that there is no continuous Ni film remaining at the interface. All interfacial nickel has segregated to NiS_x grains which sometimes extend through the whole film thickness. The

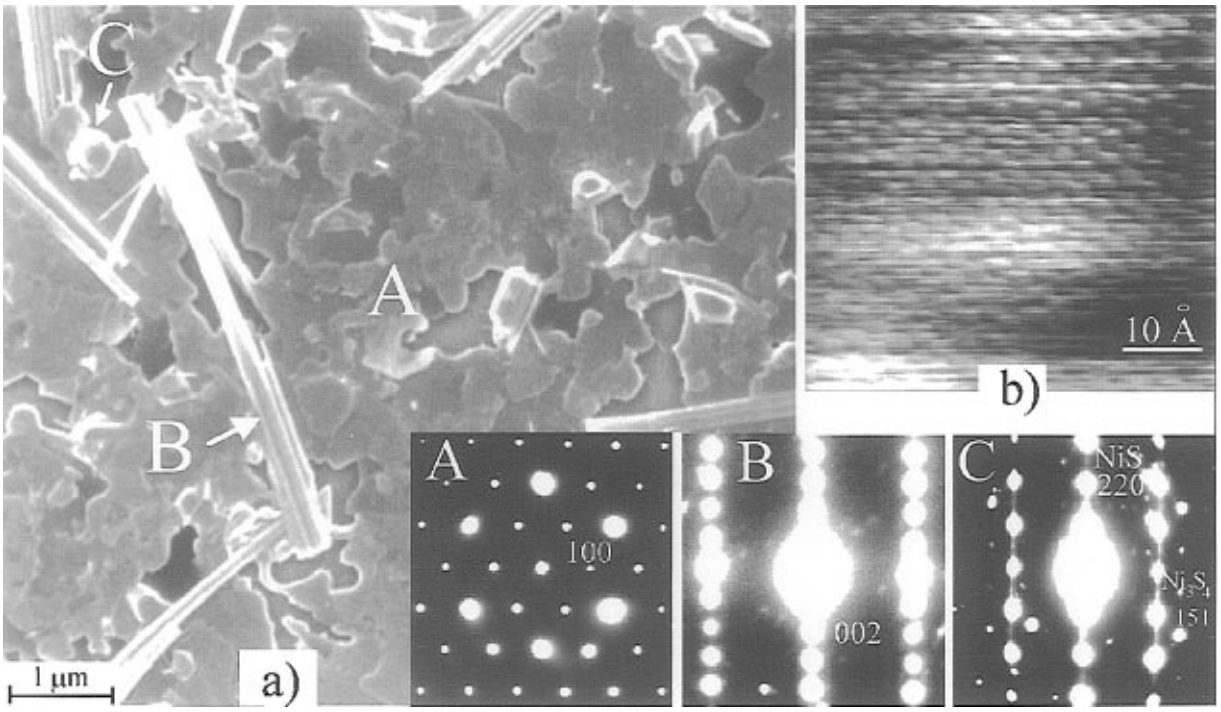

Figure 1. (a) WS_2 thin films. SEM images showing the WS_2 phase (A), tungsten oxide crystallites (B), and NiS_x grains (C). All three phases are clearly identified from their TEM diffraction pattern, shown as A, B, and C inserts. (b) Atomic STM resolution on the WS_2 crystallite of an annealed WS_3/Ni film. No filtering is applied. The image is taken in constant-current mode (sample grounded, $V_{tip} = +0.1$ V, $I_{tunnel} = 2$ nA).

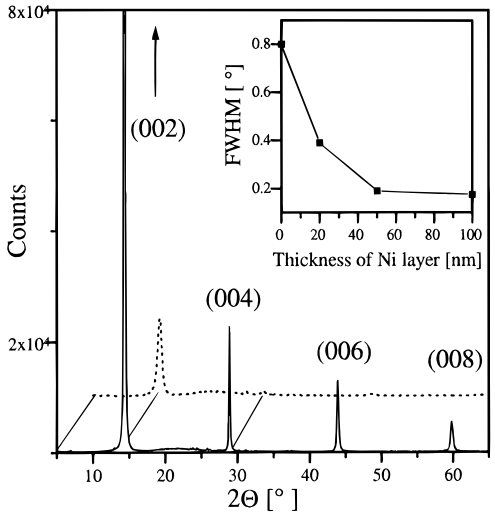

Figure 2. XRD patterns of WS_2 thin films. One film is annealed with 10 nm Ni (solid curve). No Ni layer is used for the second film (dotted curve). The broad feature between the (002) and (004) peaks is due to the quartz substrate. Insert: fwhm of the (002) peak vs Ni layer thickness. It illustrates the improvement of the crystallisation of the film with the presence of the Ni layer.

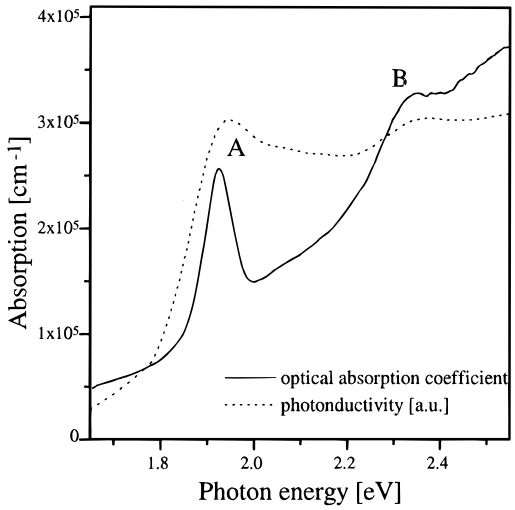

Figure 3. Absorption spectrum (solid curve) of a WS_2 thin film with A and B excitonic peaks at 1.94 and 2.36 eV. A photocurrent spectrum is also displayed (dashed curve), showing also the excitonic peaks due to higher optical absorption.

tungsten oxide phase $W_{18}O_{49}$ detected by TEM is also observed on the XRD spectra with peak heights typically 300 times smaller than the WS_2 peaks, whereas the NiS_x phases are below the detection limit of XRD. The oxide phases could be removed by KOH washing or annealing in a contaminant-free stove. This yielded, however, no noticeable change in the optoelectronic properties of the films.

The films have been characterized by optical reflection−transmission, by in-plane van der Pauw resistivity, Hall measurements, and photoconductivity measurements. The films are p-type semiconductors, with hole concentration in the $10^{17}/cm^3$ and Hall mobility in the 3−5 cm^2/V s range.

The optical absorption spectrum (Figure 3, solid curve) determined from reflection−transmission experiments at room temperature shows the same characteristic excitonic peaks A and B at 1.94 and 2.36 eV as the single crystals.[20,21] The A excitonic peak at 1.94 eV is associated with the direct optical transition of lowest energy located at the K point of the Brillouin zone.[22,23] Taking 60 meV as the binding energy of the A exciton,[24] the direct band gap of WS_2 can be located at 2.0 eV at room temperature.

The photoconductivity follows a non-linear law: $\sigma_{illum} \sim J^{\nu}$ with $\nu \sim 0.7$, where σ_{illum} is the variation of conductivity under illumination and J is the intensity of the light. The photocurrent normalized with $J^{0.7}$ is plotted in Figure 3 (dashed curve), and shows the same excitonic features (although less pronounced) as the absorption spectrum, due to enhanced photon absorption. If a quantum yield of 0.5 is assumed near the A exciton peak,[25] the mobility−recombination time product $\mu\tau$ can be estimated to be 2×10^{-3} cm^2/V, under an illumination of 20 $\mu W/cm^2$ at

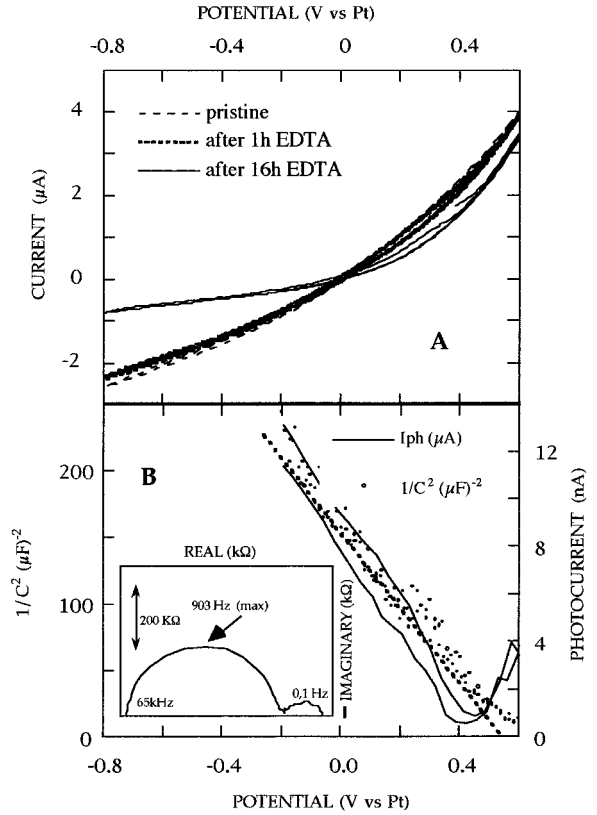

Figure 4. (A) Current−voltage curves for p-WS_2 thin film electrode (sample 85) in contact with $Fe(CN)_6^{3-/4-}$ (10 mM/10 mM) electrolyte, in the dark. Reference and counter electrode of Pt. Sample area exposed to the electrolyte 10 mm^2. Scan rate 5 mV/s. (B) Mott−Schottky plot and photocurrent as a function of the applied bias (sample 85). Mott−Schottky recorded at 2 mV/s, photocurrent at 20 mV/s scan rate. Sample area exposed to the electrolyte 10 mm^2. Insert: impedance (0.1 Hz−65 kHz) of a thin film (sample 92b) in contact with $Fe(CN)_6^{3-/4-}$ (10 mM/10 mM) electrolyte at a bias of 0 V vs Pt. Potential modulation of 10 mV. Sample area exposed to the electrolyte 10 mm^2.

a photon energy of 2 eV (these conditions correspond to a generation rate of $10^{18}/cm^3$). This indicates a diffusion length of several tens of micrometers. Under an illumination of 50 mW/cm^2, the diffusion length is of the order of a few micrometers, the typical diameter of the WS_2 crystallites. The generation of electron−hole pairs below the A peak is associated with the indirect gap of WS_2 located around 1.3 eV.[11]

(B) Photoelectrochemical Experiments. For the electrochemical experiments the standard redox couple $[Fe(CN)_6]^{3-/4-}$ was used. It has been demonstrated, in fact, that ferroferricyanide ions show fairly low affinity to chalcogenide surfaces[26,27] so that neither the oxidized nor the reduced species present a strong adsorption (such as in the case of the iodide/iodine couple). The redox potential of this couple falls within the semiconductor band gap, and the semiconductor−electrolyte junction behaves in a way similar to that of a Schottky diode. This allows fast charge transfer kinetics both in anodic and in cathodic current direction.

Typical current−potential curves obtained with TMDC film electrodes in $[Fe(CN)_6]^{3-/4-}$ are shown in Figure 4a: the rectifying character of the p-semiconductor/electrolyte junction is seen from the diode-like curve with low reverse cathodic current at negative potentials. From the slope at −0.8 V in Figure 1a (sample 85) the shunt resistance value of about 300 kΩ has been calculated for the untreated film. The samples were treated with a solution of EDTA salt for different increasing dipping times, and it was possible to see a reduction of the dark current in the reverse bias. A decrease in the cathodic dark currents has been observed previously by Parkinson et al. on n-type TMDC semiconductors[13] after treating the samples with electron-donating phosphine or isocyanide ligands and, by another approach, after treating the samples with 4-*tert*-butylpyridine. In the first case the blocking of the active reaction site was attributed to the direct binding of ligands to the metal positioned at the crystal plane edge, while in the second case a semi-intercalation mechanism was involved accompanied by electron donation from the pyridine molecules to the unsaturated metal atoms. In both cases improved power output of the cell and increased open-circuit voltage seemed to be correlated to the decrease of the dark current. The reduction in the cathodic dark currents observed by us (Figure 4a) can be attributed, therefore, to the binding of $EDTA^{2-}$ to the W atoms on the film steps, similar to that observed with isocianyde in ref 13.

In the insert of Figure 4b an electrochemical impedance measurement (FRA) at 0 V of a typical TMDC film electrode (sample 92b) is reported. The larger loop is representative for the impedance of the semiconductor space-charge region, and the smaller loop is related to the Helmholtz double layer. It is possible to represent the semiconductor space-charge region with an equivalent electrical circuit made of a capacitance (C_{sc}) in parallel with a shunt resistance due mainly to sample defects. The shunt resistance value detected from the impedance plot is 500 kΩ, of the same order of magnitude as the one calculated from the current−voltage plot in the reverse bias. The C_{sc} is 7.9 nF.

On the other hand a Mott−Schottky plot for a different electrode (sample 85, in Figure 4) gave a capacity at 0 V in the range of 10^{-8} F and a flatband potential of 0.45 V from the extrapolation to the *x*-axis. The Mott−Schottky plots drawn at different frequencies gave the same flatband, and presented some dispersion in their slope, probably due to surface states. The frequency of 200 Hz for the measurements in Figure 4b was chosen because it falls in the suitable range of frequency values indicated by the larger loop in FRA measurements.

The two independent experiments, Mott−Schottky and photovoltammetry, indicate approximately the same flatband potential value, around 0.45 V vs the redox potential (Figure 4b). This is in agreement with the flatband potential value of 0.9 V vs a saturated calomel electrode (SCE) calculated from a Mott−Schottky diagram by Cabrera for polycrystalline thin films of WS_2 in a ferro-ferricianyde electrolyte having a redox potential of +0.45 V vs SCE.[28] The value of 0.95 V vs SCE was also reported in literature for the flatband potential of single crystal p-WS_2.[29] Since the ion $EDTA^{2-}$ is negatively charged, its adsorption in the inner Helmholtz plane would possibly shift the flatband potential toward lower values. This can be useful in the case of a n-type semiconductor, because the barrier height and the depletion layer width would be increased. In the case of a p-type sample, on the contrary, a barrier reduction is expected if anion adsorption takes place overall. In fact, a large negative shift of the flatband potential was observed in our case after dipping in $EDTA^{2-}$, but only with the thin film samples having poorer photoresponse and showing no rectification in the redox electrolyte. For most samples, instead, an increase of the photocurrent under chopped light was observed as a consequence of the EDTA treatment, similar to what was previously reported for single crystals,[12] and the flatband shift was negligible.

An acceptor density (N_A) in the range of $10^{18}/cm^3$ has been determined from the slope of the plot of $1/C_{sc}^2$ vs *V* in Figure 4b. This value differs from the free hole density of $10^{17}/cm^3$

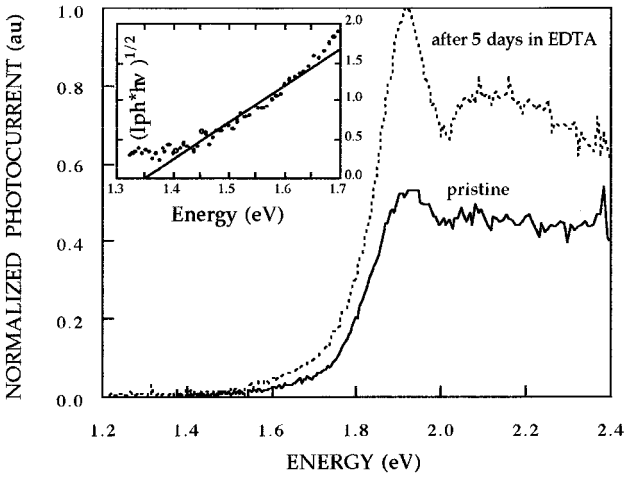

Figure 5. Photocurrent spectra of p-WS_2 thin film in contact with $Fe(CN)_6^{3-/4-}$ (10 mM/10 mM) electrolyte at an applied potential of 0 V vs Pt. The two photocurrent curves, corrected for the lamp spectral intensity, were recorded on a pristine sample and after the sample was dipped in a solution of the disodium salt of EDTA for 5 days (sample 72, area exposed 10 mm^2). Insert: indirect band gap evaluation from a photocurrent spectrum recorded at an applied potential of 0 V vs Pt (sample 85).

calculated from conductivity measurements. This difference can be explained considering that the frequency dependence of the slope of the Mott−Schottky plots introduces a certain error in the calculation of (N_A), probably attributable to the charging of surface states, so far neglected in our calculations. A lower value for C_{sc}, taking into account the surface states capacity, would yield for N_A a value somewhat closer to that calculated from conductivity.

In Figure 5 we report the photocurrent spectra for the WS_2 films, in the same cell and electrolyte as in the above experiments. From the rather large optical absorption coefficient above 1.94 eV (see Figure 3), one can calculate that most of the high-energy photons are absorbed by the film and generate free electron−hole pairs. At the exciton peak energy (where the absorption coefficient is highest), bound excitons are generated closer to the surface than free carriers. However, having a large binding energy (60 meV) such excitons are unlikely to dissociate in the space-charge electric field and eventually recombine, with a process occurring faster with less than perfect surfaces and at defects (steps and grain boundaries).[25] The photocurrent yield due to excitons must be lower, under such conditions, compared to that due to $e^- - h^+$ pairs. This is why in the photocurrent (and photoconductivity) spectra the exciton peak was always less pronounced than in the optical absorption spectra (Figures 3 and 5). Nevertheless, it has been possible to enhance the exciton peak in the photocurrent spectra (mainly with the less perfect samples) by means of a prolonged dipping of the film in EDTA (Figure 5). An increase of the photocurrent at all wavelengths has been seen for all electrodes treated with EDTA as well. Interestingly, the optical absorption spectrum of the thin films was unaffected by the EDTA treatments. The above experiments confirm that the specific absorption of ions (like $EDTA^{2-}$) modifies the surface state distribution at WS_2 and, in particular, this decreases the surface recombination of excitons.

In Figure 5 (small insert) the indirect band-gap energy of the TMDC thin films has been checked from the photocurrent spectrum at photon energy lower than 1.9 eV. Due to the low absorption coefficient in this tail, only a few photons are absorbed by the thin film and the most efficient film electrode (sample 85) needed to be used for the experiment. For this sample the photocurrent signal was almost noise free and allowed the linear fitting of the square root of the product ($I_{photocurrent}h\nu$) as a function of the photon energy, from which the band gap can be inferred in force of the linear relationship between current ($I_{photocurrent}$) and absorption coefficient.[30,31] The intercept with the energy axis gave the energy of 1.35 eV for the indirect gap, a value which is in good agreement with the data reported by Kam[25] and by Cabrera.[28]

Conclusions

So far, reports on the use for solar cells of thin layers of TMDC have been very limited, usually because a polycrystalline film of a layered semiconductor is expected to have a very high density of surface imperfections and to show very little, if any, photoeffect. In this work we have shown that it is possible to prepare thin films of WS_2, using a simple sputtering-annealing method, with the proper morphology and with optical properties close to those of single crystals. Although in-plane dark conductivity and activation energy are in the range observed for bulk materials, the nonlinear photoconductivity is an indication for the existence of light-induced trapping in this thin film material. We have formed macroscopic (10 mm^2) solid−liquid $WS_2/[Fe(CN)_6]^{3-/4-}$ junctions having a reasonably high surface barrier and showing the potential for solar cell application. The photocurrents measured at this junction are still modest and do not depend linearly on the photon flux at high light intensity, precluding the immediate use of such solid−liquid junctions in direct sunlight.

Preliminary measurements of photo-induced tunneling currents (PITC) on single grains of the same TMDC films have shown, however, excellent rectifying junction characteristics and extended linear dependence of PITC vs light intensity.[19] We can explain, therefore, our photoelectrochemical response as due to the superposition of a rather efficient junction behavior and of a sluggish lateral conduction to the Au charge collector. This conduction mechanism introduces a nonlinear photoconduction effect and a considerable cell series resistance. Further modification of the surface film composition and the improvement of the metal contacts will result, therefore, in larger photoelectrochemical currents.

The structure due to exciton transitions, a signature of the WS_2 material, was visible in all the spectra taken with the TMDC films. Enhanced recombination of excitons with respect to free electron−hole pair recombination has been measured in photocurrent spectra (and in photoconductivity). Excitons are particularly sensitive to surface defects, being generated very close to the film surface and because they can travel across the space-charge layer without dissociating. The increase of the exciton peak observed after the EDTA treatment appears to be a consequence of the selective adsorption of the EDTA ion at surface defects. Adsorption on one side may reduce the strong local electric field at such defects, and on the other side helps keeping the solvent away from the defects with its hydrophobic tail; both effects could take part in decreasing the exciton recombination rate at the electrode surface.

So far, rectifying solid-state junctions cannot be made to our WS_2 films, probably because of the presence of an excess of highly conducting NiS grains allowing short-circuit paths across (or ohmic contact to) the semiconductor material. This would suggest that the Ni layer, although playing an essential role for film crystallization, should be kept as thin as possible to avoid the formation of highly conducting phases in the film. Nevertheless, the spontaneous passivation in the redox electrolyte of such imperfections, and the additional passivation resulting from the treatment of the films with the EDTA complexing

agent, show that the semiconducting WS_2 films have the potential for large-area electronic devices.

References and Notes

(1) Spalvins, T. *J. Vac. Sci. Technol.* **1987**, *A5*, 212.
(2) Tributsch, H.; Bennett, J. C. *J. Electroanal. Chem.* **1977**, *81*, 97.
(3) Moser, J.; Bussy, F.; Levy, F. *J. Vac. Sci. Technol.* **1994**, *A12*, 494.
(4) Regula, M.; Ballif, C.; Moser, J. H.; Lévy, F. *Thin Solid Films* **1996**, *280*, 67.
(5) Kautek, W.; Gobretch, J.; Gerischer, H. *Ber. Bunsen-Ges. Phys. Chem.*, **1980**, *84*, 1034.
(6) Lewerenz, H. J.; Heller, A.; Disalvo, F. *J. Am. Chem. Soc.* **1980**, *102*, 1877.
(7) White, H. S.; Fan, F. F.; Bard, A. J. *J. Electrochem. Soc.* **1981**, *128*, 1045.
(8) Santiago, Y.; Cabrera, C. R. *J. Electrochem. Soc.* **1994**, *141*, 629.
(9) Salitra, G.; Hodes, G.; Klein, E.; Tenne, R. *Thin Solid Films* **1994**, *245*, 180.
(10) Ballif, C.; Regula, M.; Schmid, P. E.; Remskar, M.; Sanjinés, R.; Lévy, F. *App. Phys. A* **1996**, *62*, 543.
(11) Baglio, J.; Calabrese, C.; Kamieniecki, E.; Kershaw, R.; Kubiak, C.; Ricco, A.; Wold, A.; Wrighton, M.; Zoski, G. *J. Electrochem. Soc.* **1982**, *129*, 1461.
(12) Razzini, G.; Peraldo Bicelli, L.; Pini, G.; Scrosati, B. *J. Electrochem. Soc.* **1981**, *128*, 2134.
(13) Parkinson, B. A.; Furtak, T. E.; Canfield, D.; Kan, K. K.; Kline, G. *Faraday Discuss. Chem. Soc.* **1980**, *70*, 233.
(14) Levy-Clement, C.; Tenne, R. In *Photoelectrochemistry and Photovoltaics of Layered Semiconductors*; Aruchamy, A., Ed.; Kluwer Academic Publishers: 1992; p 167.
(15) Tenne, R.; Wold, A. *Appl. Phys. Lett.* **1985**, *47*, 707.
(16) Mahalu, D.; Margulis, L.; Wood, A.; Tenne, R. *Phys. Rev. B* **1992**, *45*, 1943.
(17) Tenne, R.; Galun, E.; Ennaoui, A.; Fiechter, S.; Ellmer, K.; Kunst, M.; Koelzow, Ch.; Pettenkofer, Ch.; Tiefenbacher, S. *Thin Solid Films* **1996**, *272*, 38.
(18) Regula, M.; Ballif, C.; Remskar, M.; Lévy, F. Submitted for publication in *J. Vac. Sci. Technol. A*, **1996**.
(19) EURO-TMDC, JOULE II Project, Final Report, March 1996.
(20) Wilson, J.; Yoffe, A. *Adv. Phys.* **1969**, *18*, 193.
(21) Beal, A.; Knights, J.; Liang, W. *J. Phys. C: Solid State Phys.* **1972**, *5*, 3540.
(22) Sourisseau, C.; Fouassier, M.; Alba, M.; Ghorayeb, A.; Gorochov, O. *Mater. Sci. Eng.* **1989**, *B3*, 119.
(23) Coehoorn, R.; Hass, C.; de Groot, R. A. *Phys. Rev. B* **1987**, *35*, 6203.
(24) Beal, A.; Liang, W. *J. Phys. C: Solid State Phys.* **1976**, *9*, 2459.
(25) Kam, K. K.; Parkinson, B. *J. Phys. Chem.* **1982**, *86*, 463.
(26) Tenne, R. *J. Electrochem. Soc.* **1983**, *130*, 2163.
(27) Tributsch, H. In *Photoelectrochemistry and Photovoltaics of Layered Semiconductors*; A., Aruchamy, Ed.; Kluwer Academic Publishers: 1992; p 95.
(28) Cabrera, C. R.; Abruña, H. D. *J. Electrochem. Soc.* **1988**, *135*, 1436.
(29) Baglio, J. A.; Calabrese, G. S.; Harrison, D. J.; Kamieniecki, E.; Ricco, A. J.; Wrighton, M. S.; Zosky, G. D. *J. Am. Chem. Soc.* **1983**, *105*, 2246.
(30) Gärtner, W. W. *Phys. Rev.* **1959**, *116*, 84.
(31) Butler, M. L. *J. Appl. Phys.* **1977**, *48*, 1914.